

Photoabsorption cross section in the low- x and low- Q^2 domain, and DGLAP evolution

G.R. Boroun

Department of Physics, Razi University, Kermanshah 67149, Iran

M. Kuroda

Center for Liberal Arts, Meijigakuin University, Yokohama, Japan

Dieter Schildknecht

Fakultät für Physik, Universität Bielefeld, D-33501 Bielefeld, Germany

Abstract

The behavior of the gluon distribution of the proton in the low- x , low- Q^2 domain of deep inelastic electron-proton scattering (DIS) is being investigated. By considering two-gluon exchange as the dominant interaction in the low- x , low- Q^2 domain, we imply the well-known result of scaling of the photoabsorption cross section in terms of the scaling variable $\eta(W^2, Q^2)$. From this, we derive a reliable result for the gluon distribution at the leading order of the perturbative QCD improved parton model, based on evolution from a starting scale of $Q_0^2 \cong 2 \text{ GeV}^2$. The validity of evolution, when considering its quantitative modification at low- Q^2 without any alteration at larger values of Q^2 , leads to a quantitative improvement in the extraction of the gluon distribution based on evolution from a starting scale of Q^2 conventionally chosen as $Q^2 = Q_0^2 \cong 2 \text{ GeV}^2$.

1. INTRODUCTION

The extraction of parton distribution functions (PDF's) [1–4] in the low- x , low- Q^2 domain¹, in particular, with the determination of the gluon distribution from measurements of deep inelastic scattering (DIS) in electron-proton scattering experiments [5] is interesting. The usually employed procedure rests on the choice of a "starting scale", Q_0^2 , at which a reasonable ansatz for the PDF's, in particular for the gluon density as a function of x , containing a number of free parameters, is adopted [1–3]. Upon being evolved to a value of $Q^2 \gtrsim Q_0^2$, and upon fit to the measured proton structure function at $Q^2 > Q_0^2$, the above-mentioned free parameters in the ansatz at the starting scale Q_0^2 are fixed.² The result on the input distribution at $Q^2 = Q_0^2$, as emphasized by Pelicer et al., in ref.[6], obtained by different collaborations differs significantly rather than being identical (within allowed small errors due to different fitting methods). The fits are considered not to be satisfactory (compare to ref.[6]). It seems worth noting that the resulting distribution at the input scale Q_0^2 does not obey any constraint in addition to fulfilling the only and single purpose of determining the PDF's at values of $Q^2 \gtrsim Q_0^2$; e.g., in particular, the Q_0^2 input distribution in general differs significantly from the distribution required for a representation of the measured proton structure function at $Q^2 \cong Q_0^2$. The input distribution taken by itself is devoid of any physical significance.

Our approach to the extraction of a reliable gluon distribution, to be elaborated upon in the present paper, is an entirely different one. Our starting point is the (known) observation that DIS in the low- x , low- Q^2 domain is dominated by two-gluon exchange to the (imaginary part of the) virtual Compton scattering amplitude.

The color-gauge-invariant ansatz for the two-gluon exchange amplitude leads to a quantitative description of the experimental result for the (virtual) photoabsorption cross section $\sigma_{\gamma^*p}(W^2, Q^2)$ in terms of the low- x scaling variable [7],

$$\eta(W^2, Q^2) = \frac{Q^2 + m_0^2}{\Lambda_{sat}^2(W^2)}, \quad (1.1)$$

i.e.

$$\sigma_{\gamma^*p}(W^2, Q^2) = \sigma_{\gamma^*p}(\eta(W^2, Q^2)). \quad (1.2)$$

In (1.1), $\Lambda_{sat}^2(W^2)$ increases as a small power of W^2 , and $m_0^2 < m_\rho^2$, where m_ρ denote the ρ -meson mass. Compare to Fig.2 [8] and Section 2 for the $\eta(W^2, Q^2)$ dependence of the photoabsorption cross section.

¹ In conventional notation, Q^2 denotes the negative of the photon virtuality, and x the Bjorken variable $x \cong Q^2/W^2$, where W^2 refers to the photon-proton total energy squared.

² The procedure allows one to include various different values of Q^2 within the single "global fit" in terms of the x -dependence at the Q_0^2 starting scale. The error bars of the fit are considerably reduced compared to a fit restricted to a single value of Q^2 .

The proton structure function corresponding to $\sigma_{\gamma^*p}(\eta(W^2, Q^2))$ will subsequently be used to derive the (dominant) gluon distribution. Compare to Section 3. The accuracy and reliability of the extracted gluon distribution in the low- x , low- Q^2 domain at leading order of the pQCD improved parton model will only be restricted by measurement errors and the associated reliability of the photoabsorption cross section in terms of $\eta(W^2, Q^2)$.

The evolution of the proton structure function $F_2(x, Q^2)$ corresponding to $\sigma_{\gamma^*p}(\eta(W^2, Q^2))$ is examined in Section 4. Standard evolution holds for $\eta(W^2, Q^2) \gtrsim 1$, i.e. for fairly large values of Q^2 , while requiring an explicitly quantitatively determined deviation for $\eta \lesssim 1$. Compare to Section 4.

2. BASIC ASSUMPTIONS OF THE COLOR-DIPOLE PICTURE(CDP) AND DERIVATION OF THE $\eta(W^2, Q^2)$ DEPENDENCE

It will be useful to work in the proton rest frame. The photon undergoes three-momentum conserving, energy-non-conserving transitions to on-shell $q\bar{q}$ states of finite mass, $M_{q\bar{q}}$ ³, and sufficiently long life time to interact with the proton.

Consistency between the Q^2 dependence from e^+e^- annihilation (entering the $\gamma^*(q\bar{q})$ transition) and e^-p scattering in the framework of the underlying dispersion relation [9] led to requiring opposite signs of interacting $q\bar{q}$ states neighboring in mass $M_{q\bar{q}}$ known as "off-diagonal generalized vector dominance"[10]. In the framework of QCD, this opposite sign between contributions from neighboring states is recognized [11] as a property of the color-gauge-invariant interaction of $q\bar{q}$ states with the proton via the structure of two-gluon couplings. Upon transition to the transverse distance between quark and antiquark, \vec{r}_\perp , one arrives at what is known as the "Color Dipole Picture (CDP)" [7, 11].

The basic assumption is the color-gauge invariant representation for the dipole interaction resulting from two-gluon exchange [8, 11],

$$\sigma_{(q\bar{q})p}(\vec{r}_\perp, z(1-z), W^2) = \int d^2\vec{\ell}_\perp \tilde{\sigma}(\vec{\ell}_\perp^2, z(1-z), W^2)(1 - e^{-i\vec{\ell}_\perp \vec{r}_\perp}), \quad (2.1)$$

entering

$$\sigma_{\gamma_{L,T}^*p}(W^2, Q^2) = \int dz \int d^2\vec{r}_\perp \left| \Psi_{L,T}(\vec{r}_\perp^2, z(1-z), Q^2) \right|^2 \sigma_{(q\bar{q})p}(\vec{r}_\perp, z(1-z), W^2). \quad (2.2)$$

We note tht the color-gauge-invariant representation (2.1) by itself is sufficient [8] to derive the low- $\eta(W^2, Q^2)$ scaling behavior,

$$\sigma_{\gamma^*p}(W^2, Q^2) = \sigma_{\gamma^*p}(\eta(W^2, Q^2)), \quad (2.3)$$

with $\Lambda_{sat}^2(W^2)$ being given by

$$\Lambda_{sat}^2(W^2) = \frac{\int d\vec{\ell}_\perp^2 \tilde{\sigma}_{(q\bar{q})_L^{I=1p}}(\vec{\ell}_\perp^2, W^2)}{\int d\vec{\ell}_\perp^2 \tilde{\sigma}_{(q\bar{q})_L^{I=1p}}(\vec{\ell}_\perp^2, W^2)}, \quad (2.4)$$

$$\vec{\ell}_\perp^2 \equiv \frac{\vec{\ell}_\perp^2}{z(1-z)},$$

as well as the low- η and the large- η dependence of the photoabsorption cross section,

$$\sigma_{\gamma^*p}(W^2, Q^2) = \sigma_{\gamma^*p}(\eta(W^2, Q^2)) = \frac{\alpha}{\pi} \sum_q Q_q^2 \begin{cases} \sigma_T^{(\infty)}(W^2) \ln \frac{1}{\eta(W^2, Q^2)} & , \quad \eta \ll 1, \\ \frac{1}{6}(1+2\rho)\sigma_L^{(\infty)}(W^2) \frac{1}{\eta} & , \quad 1 \ll \eta \lesssim 40. \end{cases} \quad (2.5)$$

In (2.5),

$$\sigma_T^{(\infty)}(W^2) = \pi \int d\vec{\ell}_\perp^2 \tilde{\sigma}_{(q\bar{q})_T^{I=1p}}(\vec{\ell}_\perp^2, W^2) = \rho \sigma_L^{(\infty)}(W^2) = \rho \pi \int d\vec{\ell}_\perp^2 \tilde{\sigma}_{(q\bar{q})_L^{I=1p}}(\vec{\ell}_\perp^2, W^2), \quad (2.6)$$

³ See e.g. Ref.[12] for a concise review of the well-known point

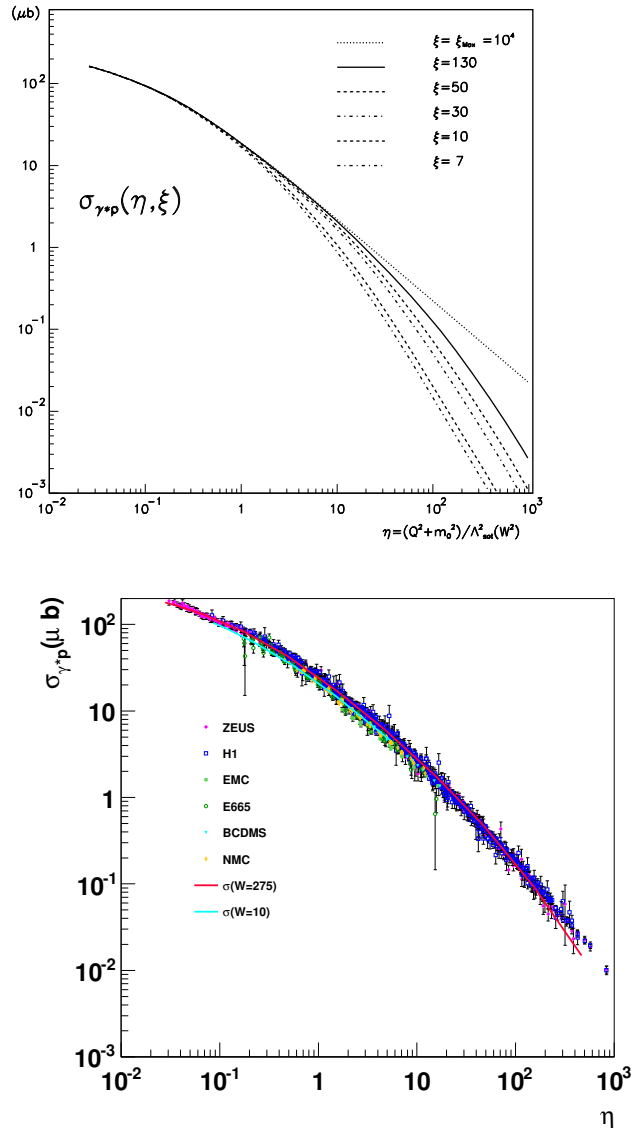


FIG. 1. The theoretical results for the photoabsorption cross section $\sigma_{\gamma^*p}(\eta(W^2, Q^2), \xi)$ in the CDP as a function of the low-x scaling variable $\eta(W^2, Q^2) = (Q^2 + m_0^2)/\Lambda_{sat}^2(W^2)$ for different values of the parameter ξ that determines the (squared) mass range $M_{q\bar{q}}^2 \leq m_1^2(W^2) = \xi \Lambda_{sat}^2(W^2)$ of the $\gamma^* \rightarrow q\bar{q}$ fluctuations that are taken into account. The experimental results for $\sigma_{\gamma^*p}(\eta(W^2, Q^2), \xi)$ (lower panel) lie on the full line corresponding to $\xi = \xi_0 = 130$, compare to ref. [8].

where $\sigma_T^{(\infty)}(W^2)$ and $\sigma_L^{(\infty)}(W^2)$ are weakly W^2 -dependent cross section for $(q\bar{q})_{T,L}$ -proton scattering of hadronic size. A preferable value of ρ in (2.6) is given by $\rho = \frac{4}{3}$. The weakly W^2 dependent cross section (2.6) is related to and is replaced by reliable independent fits to $Q^2 = 0$ photoproduction. The factor ρ in (2.6), via $R(W^2, Q^2) = 1/2\rho$ determines the longitudinal-to transverse ratio, $R(W^2, Q^2)$ of the photoabsorption cross section $\sigma_{\gamma^*p}(\eta(W^2, Q^2))$.

Upon specification of $\tilde{\sigma}(\vec{l}_\perp^2, z(1-z), W^2)$ in (2.1) via

$$\tilde{\sigma}(\vec{l}_\perp^2, z(1-z), W^2) = \frac{\sigma^{(\infty)}(W^2)}{\pi} \delta\left(\vec{l}_\perp^2 - z(1-z)\Lambda_{sat}^2(W^2)\right), \quad (2.7)$$

one obtains the full CDP results in (2.3) shown in Fig.1. Compare to Appendix A for the derivation of the analytic

expression for $\sigma_{\gamma^*p}(\eta(W^2, Q^2))$.

The parameters entering the result in Fig.1 are given by

$$m_0^2 = 0.15\text{GeV}^2 \quad (2.8)$$

as well as

$$\begin{aligned} C_1 &= 0.31\text{GeV}^2, \\ C_2 &= 0.27, \end{aligned} \quad (2.9)$$

where⁴

$$\Lambda_{sat}^2(W^2) = C_1 \left(\frac{W^2}{1\text{GeV}^2} \right)^{C_2}. \quad (2.10)$$

The results may equivalently be expressed in terms of the proton structure function

$$F_2(W^2, Q^2) = \frac{Q^2}{4\pi^2\alpha} (\sigma_{\gamma_T^*p}(W^2, Q^2) + \sigma_{\gamma_L^*p}(W^2, Q^2)) = \frac{Q^2}{4\pi^2\alpha} \sigma_{\gamma^*p}(\eta(W^2, Q^2)). \quad (2.11)$$

We note the range of $\eta(W^2, Q^2)$ for the value of $Q^2 = 1.9\text{GeV}^2$ and presently relevant values of $W^2 = 10^3 \text{ GeV}^2$ to $W^2 = 10^5\text{GeV}^2$ that is given by

$$0.30 \lesssim \eta(W^2, Q^2) \lesssim 1.03. \quad (2.12)$$

The parameter ξ also used in Fig.1 yields the mass range of $q\bar{q}$ transitions,

$$M_{q\bar{q}}^2 \leq m_1^2 = \xi \Lambda_{sat}^2(W^2). \quad (2.13)$$

The finite value of ξ only becomes relevant for $\eta(W^2, Q^2) \gtrsim 10$. For $\eta(W^2, Q^2) \lesssim 10$, ξ may be put to $\xi = \infty$. In the transition to small $\eta(W^2, Q^2)$, i.e. small Q^2 , the transition of the photon to large values of $M_{q\bar{q}}$ dies out. Compare to Fig.1.

3. THE GLUON DISTRIBUTION FUNCTION

In leading order of pQCD, the longitudinal structure function, $F_L(x, Q^2)$, as a consequence of the dominance of the gluon distribution at low- x , is determined by [13]

$$F_L(x, Q^2) = \frac{2\alpha_s(Q^2)}{\pi} \left(\sum_q Q_q^2 \right) I_g(x, Q^2), \quad (3.1)$$

where $I_g(x, Q^2)$ denotes an integral over the gluon distribution,

$$I_g(x, Q^2) = \int_x^1 \frac{dy}{y} \left(\frac{x}{y} \right)^2 \left(1 - \frac{x}{y} \right) G(y, Q^2). \quad (3.2)$$

For a considerable range of gluon distributions, $G(y, Q^2)$, the integral in 3.2 may be replaced by the simple proportionality

$$F_L(\xi_L x, Q^2) = \frac{\alpha_s(Q^2)}{3\pi} \left(\sum_q Q_q^2 \right) G(x, Q^2), \quad (3.3)$$

where the shift parameter $x \rightarrow \xi_L x$ on the left-hand side in (3.3) has the preferred value of $\xi_L \cong 0.40$ [13].

The CDP result for the longitudinal structure function is compared to available experimental results in Fig.2.

⁴ Validity of evolution at large Q^2 implies the constraint $C_2 = 0.29$ consistent with experiment. See Appendix B for this known restriction on the exponent C_2 that reduces the fitted parameters to m_0^2 and the normalization C_1 .

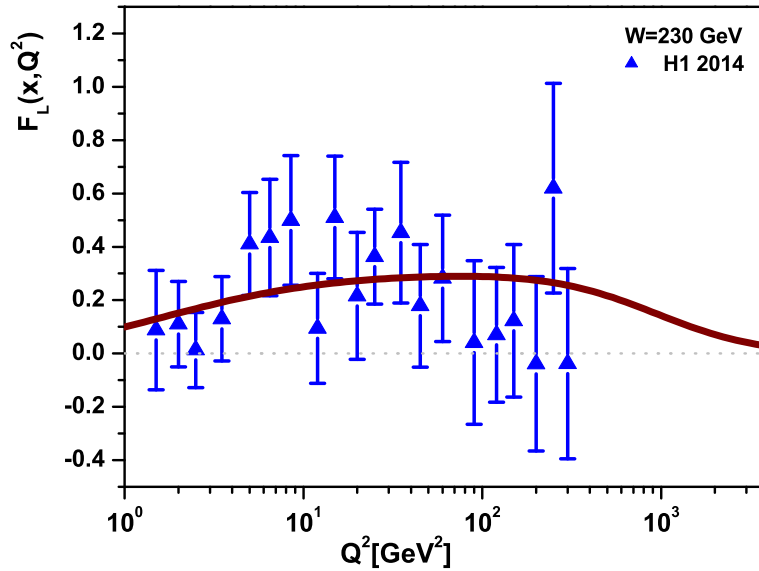


FIG. 2. Experimental data [14] and the CDP prediction of $F_L(x, Q^2)$ are compared.

	$W^2 = 10^5$ [GeV ²]	$W^2 = 10^4$ [GeV ²]	$W^2 = 10^3$ [GeV ²]
$Q^2 = 100$ [GeV ²]	1.043	1.037	0.981
$Q^2 = 50$ [GeV ²]	1.041	1.037	1.012
$Q^2 = 10$ [GeV ²]	1.035	1.035	1.030
$Q^2 = 2$ [GeV ²]	1.021	1.026	1.029
$Q^2 = 1$ [GeV ²]	1.015	1.021	1.026

TABLE I. The table shows the ratio of $F_L(W^2, Q^2)$ in (3.1) to $F_L(W^2, Q^2)$ from the CDP, where the former is calculated by inserting $G(x, Q^2)$ obtained from (3.3) by using $F_L(W^2, Q^2)$ from the CDP.

Substitution of the CDP result for $F_L(\xi_L x, Q^2)$ into (3.3) allows one to determine the gluon distribution, $G(x, Q^2)$, in terms of $F_L(\xi_L x, Q^2)$. The accuracy of the gluon distribution resulting from $F_L(\xi_L x, Q^2)$ is tested by insertion of $G(x, Q^2)$ obtained from (3.3) into the integral in (3.1).

The resulting $F_L(x, Q^2)$ agrees with the input for $F_L(x, Q^2)$ within less than 4%, compare to Table 1. The gluon distribution obtained from (3.3) for $1 \text{ GeV}^2 \lesssim Q^2 \lesssim 100 \text{ GeV}^2$ and $10^3 \text{ GeV}^2 \lesssim W^2 \lesssim 10^5 \text{ GeV}^2$ indeed reproduces $F_L(x, Q^2)$ in (3.1).

The derived gluon distribution is relevant for $Q^2 \gtrsim Q_0^2$, where Q_0^2 must be large enough to allow for $\alpha_s(Q^2) \ll 1$. Our method of determining the gluon distribution at leading order of pQCD from the successful fits to the experimental results for the proton structure functions in the CDP yields unambiguous and reliable results for the gluon distribution of the proton at low- x and chosen values of Q^2 . Indeed, evaluation of the pQCD result for $F_L(x, Q^2)$ in (3.1) in terms of the extracted gluon distribution reproduces the experimentally determined longitudinal structure function of the proton, see Table I.

4. EVOLUTION

We turn to examining evolution, i.e. studying the logarithmic derivative $\frac{\partial F_2(x, Q^2)}{\partial \ln Q^2}$ of the experimentally determined structure function $F_2(x, Q^2)$.

In the low- x , low- Q^2 domain of the pQCD improved parton model for $Q^2 \gg 1 \text{ GeV}^2$, at leading order, DIS is dominated by the gluon distribution $G(x, Q^2)$. Both $F_L(x, Q^2)$ as well as $\frac{\partial F_2(x, Q^2)}{\partial \ln Q^2}$ are related to $G(x, Q^2)$ by integrals of similar magnitude [13],

$$\begin{aligned} F_L(x, Q^2) &= \frac{2\alpha_s(Q^2)}{\pi} \int_x^1 \frac{dy}{y} \left(\frac{x}{y}\right)^2 \left(1 - \frac{x}{y}\right) G(y, Q^2) \\ &\cong \frac{10\alpha_s(Q^2)}{27\pi} G\left(\frac{x}{\xi_L}, Q^2\right) \end{aligned} \quad (4.1)$$

with

$$\frac{1}{\xi_L} = \frac{1}{0.4} = 2.5, \quad (4.2)$$

and [15]

$$\begin{aligned} \frac{\partial F_2(x, Q^2)}{\partial \ln Q^2} &= \frac{5\alpha_s}{9\pi} \int_0^{1-x} dz \left((1-z)^2 + z^2\right) G\left(\frac{x}{1-z}, Q^2\right) \\ &\cong \frac{10\alpha_s(Q^2)}{27\pi} G\left(\frac{x}{\xi_2}\right), \end{aligned} \quad (4.3)$$

where

$$\frac{1}{\xi_2} = \frac{1}{0.5} = 2.0. \quad (4.4)$$

According to (4.3) and (4.1),

$$\begin{aligned} \frac{\partial F_2(x, Q^2)}{\partial \ln Q^2} &= F_L\left(\frac{\xi_L}{\xi_2}x, Q^2\right) \\ &\cong F_L(x, Q^2), \end{aligned} \quad (4.5)$$

where the shift factor $\frac{\xi_L}{\xi_2} = 0.8$ was approximated by $\frac{\xi_L}{\xi_2} = 1$ in the second step of (4.5). In the pQCD improved parton model, in terms of the underlying gluon distribution, evolution (4.5) is recognised as a consequence of the proportionalities (4.1) and (4.3).

In distinction from the pQCD improved parton model, where the range of Q^2 in (4.1) and (4.3) must be restricted to sufficiently large values of $Q^2 \gg 1 \text{ GeV}^2$, in the CDP the representation of the measured photoabsorption cross section $\sigma_{\gamma^*p}(\eta(W^2, Q^2))$ and the associated structure function include the transition to low Q^2 , including the $Q^2 = 0$ photoproduction limit. The CDP allows one to quantitatively analyze the magnitude of the potential deviation from DGLAP evolution, when passing from the validity of standard evolution at large Q^2 to the low- Q^2 domain.

Differentiation of $F_2(x, Q^2)$ in (2.11), upon replacing W^2 by $W^2 = \frac{Q^2}{x}$, and simplifying the notation via

$$\sigma_{\gamma_T^*p}(x, Q^2) = \sigma_T, \quad \sigma_{\gamma_L^*p}(x, Q^2) = \sigma_L, \quad (4.6)$$

leads to

$$\begin{aligned} \frac{\partial F_2(x, Q^2)}{\partial \ln Q^2} &= F_L(x, Q^2) \left(1 + \frac{\sigma_T}{\sigma_L} + \frac{Q^2}{\sigma_L} \frac{\partial}{\partial Q^2} (\sigma_T + \sigma_L)\right) \\ &\equiv F_L(x, Q^2) R_3(x, Q^2), \end{aligned} \quad (4.7)$$

Comparison of (4.7) and the second line of (4.5) shows that $R_3(x, Q^2)$ indeed quantifies deviations from DGLAP evolution ($R_3(x, Q^2) = 1$), when passing from the large- Q^2 validity to the low- Q^2 domain.

Equation (4.7) is evaluated by substitution of the CDP results given in Appendix A, i.e.

$$F_L(x, Q^2) = \frac{Q^2}{4\pi^2\alpha} \frac{\sigma_{\gamma p}(W^2)}{\left(\ln \frac{\rho}{\mu(W^2)}\right)} I_L^{(1)}(\eta, \mu), \quad (4.8)$$

and $R_3(x, Q^2)$ is given by

$$R_3(x, Q^2) = \frac{1}{I_L^{(1)}(\eta, \mu)} \left[I_T^{(1)}\left(\frac{\eta}{\rho}, \frac{\mu}{\rho}\right) + I_L^{(1)}(\eta, \rho) + \frac{\partial}{\partial \ln Q^2} \left(I_T^{(1)}\left(\frac{\eta}{\rho}, \frac{\mu}{\rho}\right) + I_L^{(1)}(\eta, \rho) \right) \right], \quad (4.9)$$

where

$$\begin{aligned} I_L^{(1)}(\eta, \mu) &= \frac{\eta^{-\mu}}{\eta} (1 - 2\eta I_0(\eta)), \\ I_T^{(1)}(\eta, \mu) &= I_0(\eta) - \frac{\eta^{-\mu}}{\eta} (1 - 2\eta I_0(\eta)), \end{aligned} \quad (4.10)$$

with

$$I_0(\eta) = \frac{1}{\sqrt{1+4\eta}} \ln \frac{\sqrt{1+4\eta}+1}{\sqrt{1+4\eta}-1}. \quad (4.11)$$

The results for $R_3(x, Q^2)$ as a function of Q^2 for various choices of x are presented in Fig.3. At large Q^2 , $R_3(x, Q^2)$ converges towards unity, $R_3(x, Q^2) = 1$, corresponding to validity of standard evolution according to (4.5) and (4.7).

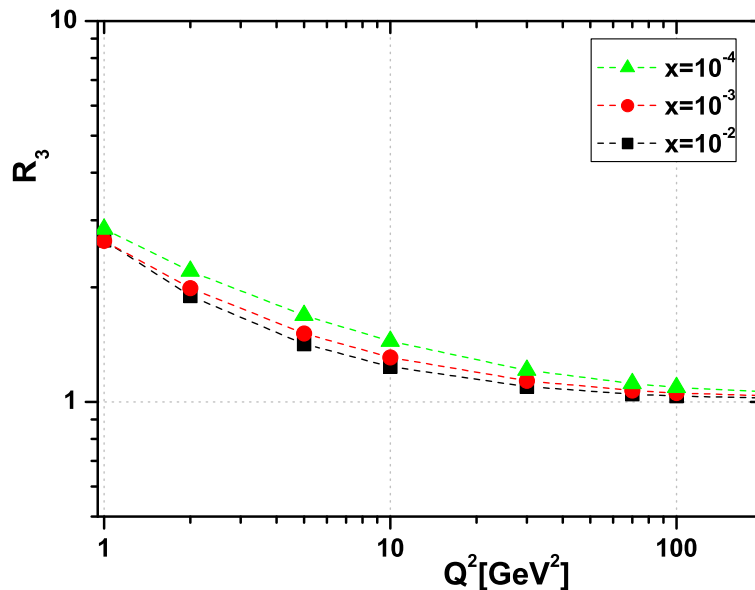


FIG. 3. The factor $R_3(x, Q^2)$ in (4.7), multiplying $F_L(x, Q^2)$ in the CDP, as a function of Q^2 at fixed values of x .

For low values of Q^2 , in Fig.3, one observes an increasingly stronger rise of $R_3(x, Q^2)$ corresponding to a correction factor to standard evolution that is given by $R_3(x, Q^2)$.

The increase of $R_3(x, Q^2)$ with decreasing Q^2 may be directly visualized as a multiplicative factor to $\sigma_{\gamma^* p}(\eta(W^2, Q^2))$. Indeed [16],

$$\frac{\partial F_2(x, Q^2)}{\partial \ln Q^2} = \frac{Q^2}{4\pi^2\alpha} \frac{1}{1+2\rho} \sigma_{\gamma^* p}(\eta(W^2, Q^2))_{W^2=Q^2/x} R_3(x, Q^2). \quad (4.12)$$

or

$$\sigma_{\gamma^*p}(\eta(W^2, Q^2)_{W^2=Q^2/x}) = \frac{\partial F_2(x, Q^2)}{\partial \ln Q^2} \frac{4\pi^2\alpha}{Q^2} (1 + 2\rho) \frac{1}{R_3(x, Q^2)}. \quad (4.13)$$

In Fig.4, we show the result for $\sigma_{\gamma^*p}(\eta(W^2, Q^2))$ from Fig.1, along with the impact of multiplying by $R_3(x, Q^2)$. It is evident that a factor of $1/R_3(x, Q^2)$ in Eq. (4.13), where $R_3(x, Q^2)$ is defined in Eq. (4.9), which is different from unity, must be applied to the evolution prediction at low Q^2 ($\eta \lesssim 1$) to achieve consistency between evolution and the experimental results. The experimental data, represented by the $\eta(W^2, Q^2)$ -dependence in Fig.1 from the CDP, satisfy evolution ($R_3(x, Q^2) = 1$). The discrepancy between the experimental data (black-solid curve) and the DGLAP evolution (red-dashed curve) at low η indicates that the relatively low initial scale used in many global analyses to extract proton PDFs is too low, and the DGLAP evolution cannot be relied upon in that region. By using η , we observe a large η behavior as $1/\eta$ and a deviation from $1/\eta$ for η less than 1. Since DGLAP implies $1/\eta$, this principle is violated at a scale of approximately $\simeq 1.9 \text{ GeV}^2$. Therefore, $Q^2 \simeq 1.9 \text{ GeV}^2$ can not be used as a starting scale. The data exhibit inconsistency with evolution at low η .

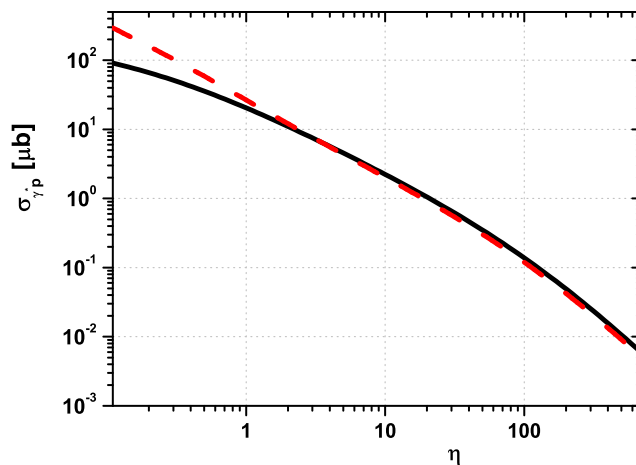


FIG. 4. The photoabsorption cross section (1.2) $\sigma_{\gamma^*p}(\eta = \frac{Q^2+m_0^2}{\Lambda_{sat}^2})$ (black curve) describing the DIS experimental results compared to $\sigma_{\gamma^*p}(\eta)R_3(x, Q^2)$ according to (4.12) (red curve).

5. CONCLUSION

Based on the dominant interaction of two-gluon exchange in photoabsorption and the associated structure functions of the proton in DIS, which implies scaling in terms of the low x scaling variable $\eta(W^2, Q^2)$, we have derived a reliable result for the gluon distribution function at the leading order of pQCD in the low- x , low- Q^2 domain. The DGLAP evolution is consistent with experimental results for $F_2(x, Q^2)$ in the CDP at large Q^2 . We provide explicit quantitative results for its necessary modification at low Q^2 , including the behavior as Q^2 approaches very low values towards $Q^2 = 0$. With this modification, the evolution is applicable to experimental data of DIS in the CDP at any Q^2 in the low- x , low- Q^2 domain.

Our results suggest a method for determining of the gluon distribution by evolving from a given starting scale Q^2 approximately $Q_0^2 \cong 2 \text{ GeV}^2$. The assumed value at the starting scale should be supplemented by the experimentally determined DIS result for the structure function at the value of Q_0^2 . Evolution of the structure function from Q_0^2 to

$Q^2 \gtrsim Q_0^2$, using the mentioned low Q^2 modification, will lead to a successful result for the structure function at large Q^2 and a reliable result for the associated gluon distribution.

APPENDIX A. ANALYTIC EXPRESSION FOR $\sigma_{\gamma^*p}(W^2, Q^2)$ AND FOR $F_L(x, Q^2)$ IN THE CDP.

The transverse and longitudinal photoabsorption cross section in CDP is given by [8]

$$\sigma_{\gamma_{L^*}p}(W^2, Q^2) = \frac{\alpha R_{e^+e^-}}{3\pi} \sigma^{(\infty)}(W^2) I_L(\eta(W^2, Q^2), \mu(W^2)) G_L(u). \quad (\text{A.1})$$

$$\sigma_{\gamma_{T^*}p}(W^2, Q^2) = \frac{\alpha R_{e^+e^-}}{3\pi} \sigma^{(\infty)}(W^2) I_T\left(\frac{\eta(W^2, Q^2)}{\rho}, \frac{\mu(W^2)}{\rho}\right) G_T(u), \quad (\text{A.2})$$

where

$$\mu(W^2) = \eta(W^2, 0) = \frac{m_0^2}{\Lambda_{sat}^2(W^2)}. \quad (\text{A.3})$$

In (A.1) and (A.2), $R_{e^+e^-} = 3 \sum_q Q_q^2$, where the sum runs over the actively contributing quark flavors, and Q_q denotes the quark charge, while $G_T(u)$ and $G_L(u)$ are correction factors due to the finite value of ξ with

$$u = \frac{\xi}{\eta}. \quad (\text{A.4})$$

The quantity $\rho = \frac{4}{3}$ is the ratio of the size of the $(q\bar{q})$ dipole in the transverse and longitudinal amplitude, which signifies the enhancement of dipole size in the transverse amplitude. It turns out that the relevant region of $\mu(W^2)$ fulfills the bound $\mu(W^2) < 1$. Under this assumption $I_{L,T}(\eta(W^2, Q^2), \mu(W^2))$ becomes

$$I_{L,T}(\eta(W^2, Q^2), \mu(W^2)) = I_{L,T}^{(1)}(\eta(W^2, Q^2), \mu(W^2)) (1 + 0(\mu(W^2))), \quad (\text{A.5})$$

where $I_L^{(1)}(\eta(W^2, Q^2), \mu(W^2))$ and $I_T^{(1)}(\eta(W^2, Q^2), \mu(W^2))$ are given by

$$I_L^{(1)}(\eta, \mu) = \frac{\eta - \mu}{\eta} \times \left(1 - \frac{\eta}{\sqrt{1+4(\eta-\mu)}} \ln \frac{\eta(1 + \sqrt{1+4(\eta-\mu)})}{4\mu - 1 - 3\eta + \sqrt{(1+4(\eta-\mu))((1+\eta)^2 - 4\mu)}} \right), \quad (\text{A.6})$$

$$I_T^{(1)}(\eta, \mu) = \frac{1}{2} \ln \frac{\eta - 1 + \sqrt{(1+\eta)^2 - 4\mu}}{2\eta} - \frac{\eta - \mu}{\eta} + \frac{1 + 2(\eta - \mu)}{2\sqrt{1+4(\eta-\mu)}} \times \ln \frac{\eta(1 + \sqrt{1+4(\eta-\mu)})}{4\mu - 1 - 3\eta + \sqrt{(1+4(\eta-\mu))((1+\eta)^2 - 4\mu)}}. \quad (\text{A.7})$$

We note the photoproduction ($Q^2 = 0$) limit of (A.2),

$$\sigma_{\gamma p}(W^2) \equiv \lim_{\eta \rightarrow \mu} \sigma_{\gamma_{T^*}p}(W^2, Q^2) = \frac{\alpha R_{e^+e^-}}{3\pi} \sigma^{(\infty)}(W^2) G_T(u) \ln \frac{\rho}{\mu}. \quad (\text{A.8})$$

In the limit of very high energy, $\mu(W^2) \ll 1$, (A.5) may be further simplified. We note that $\mu(W^2) \leq \eta(W^2, Q^2) \leq \eta_{Max}(W^2)$, where $\eta_{Max}(W^2)$ is determined by the required restriction to low values of $x \leq x_0 \lesssim 0.1$, or $Q^2 \leq x_0 W^2$, i.e.

$$\eta(W^2, Q^2) \leq \eta_{Max}(W^2) = \frac{x_0 W^2}{\Lambda_{sat}^2(W^2)}. \quad (\text{A.9})$$

With $\mu(W^2) \ll 1$ and $\eta(W^2, Q^2) \geq \mu(W^2)$, upon making use of the identity

$$\begin{aligned} 2 \ln \frac{\sqrt{1+4\eta} + 1}{\sqrt{1+4\eta} - 1} &= \ln \frac{(1+\eta)\sqrt{1+4\eta} + 1 + 3\eta}{\eta(\sqrt{1+4\eta} - 1)} = \\ &= \ln \frac{\eta(1 + \sqrt{1+4\eta})}{(1+\eta)\sqrt{1+4\eta} - 1 - 3\eta}, \end{aligned} \quad (\text{A.10})$$

and of the definition

$$I_0(\eta) = \frac{1}{\sqrt{1+4\eta}} \ln \frac{\sqrt{1+4\eta}+1}{\sqrt{1+4\eta}-1}, \quad (\text{A.11})$$

we find that (A.5) and (A.6) become

$$\begin{aligned} I_L^{(1)}(\eta, \mu) &= \frac{\eta - \mu}{\eta} (1 - 2\eta I_0(\eta)), \\ I_T^{(1)}(\eta, \mu) &= I_0(\eta) - \frac{\eta - \mu}{\eta} (1 - 2\eta I_0(\eta)). \end{aligned} \quad (\text{A.12})$$

$\sigma^{(\infty)}(W^2)$ in (A.1) and (A.2) is evaluated from the photoproduction limit (A.8) as

$$\sigma^{(\infty)}(W^2) = \frac{3\pi}{\alpha R_{e^+e^-}} \frac{1}{\left(\ln \frac{\rho}{\mu}\right) G_T(u)} \sigma_{\gamma p}(W^2). \quad (\text{A.13})$$

Inserting (A.13) in (A.1), we obtain

$$F_L(x, Q^2) = \frac{Q^2}{4\pi^2\alpha} \sigma_{\gamma_{LP}^*}(W^2, Q^2) = \frac{Q^2}{4\pi^2\alpha} \frac{\sigma_{\gamma p}(W^2)}{\left(\ln \frac{\rho}{\mu(W^2)}\right) G_T(u)} I_L^{(1)}(\eta, \mu) G_L(u), \quad (\text{A.14})$$

Since $\xi \cong 130$, while $\eta \lesssim 40$ in the region we are interested in, we can set approximately $u = \infty$, meaning no finite ξ corection $G_L(u) = G_T(u) = 1$, to obtain

$$F_L(x, Q^2) = \frac{Q^2}{4\pi^2\alpha} \frac{\sigma_{\gamma p}(W^2)}{\left(\ln \frac{\rho}{\mu(W^2)}\right)} I_L^{(1)}(\eta, \mu) \quad (\text{A.15})$$

in (4.8) of the main text.

APPENDIX B. EVALUATION OF C_2 IN $\Lambda_{sat}^2(W^2)$

We note that in the CDP, for $x \ll 0.1$ and Q^2 sufficiently large [8], the (unmodified) evolution equation (4.3) becomes

$$\frac{\partial}{\partial \ln W^2} F_2\left(\frac{\xi_L}{\xi_2} W^2\right) = \frac{1}{2\rho_W + 1} F_2(W^2). \quad (\text{B.1})$$

We remark that the hadronic ratio of longitudinal-to transverse $(q\bar{q})_{L,T}$ p scattering, ρ_W , is at most weakly dependent on W , i.e. $\rho_W = \rho \cong \text{const} = 4/3$. Inserting

$$F_2(W^2) \propto \Lambda_{sat}^2(W^2) = C_1 \left(\frac{W^2}{1\text{GeV}^2}\right)^{C_2}, \quad (\text{B.2})$$

into (B.2), we obtain an important constraint,

$$C_2(2\rho + 1) \left(\frac{\xi_L}{\xi_2}\right)^{C_2} = 1, \quad (\text{B.3})$$

or conveniently to first order in C_2

$$C_2 \cong \frac{1}{2\rho + 1} \frac{1}{\left(1 - \frac{1}{2\rho + 1} \ln \frac{\xi_2}{\xi_L}\right)}. \quad (\text{B.4})$$

With the preferred value of $\frac{\xi_2}{\xi_L} = 1.25$ and $\rho = \frac{4}{3}$, one obtains the prediction of

$$C_2 = 0.29. \quad (\text{B.5})$$

Evolution accordingly implies the exponent of $\Lambda_{sat}^2(W^2)$ proportional to $\left(\frac{W^2}{1\text{GeV}^2}\right)^{C_2}$ consistent with its experimental determination .

-
- [1] L.A. Harland-Lang, A.D. Martin, P. Motylinski and R.S. Thorne, *Eur. Phys. J. C* **75**, 204 (2015).
 - [2] J.F. Owens, A. Accardi and W. Melnitchouk, *Phys.Rev.D* **87**, 094012 (2013).
 - [3] Richard D. Ball et al., *JHEP* **2015**, 40 (2015);
R.D. Ball et al. [NNPDF Collaboration], *Eur. Phys. J. C* **77**, 663 (2017).
 - [4] A. Buckley, J. Ferrando, S. Lloyd, K. Nordstrom, B. Page, M. Ruefenacht, M. Schoenherr and G. Watt, *Eur. Phys. J. C* **75**, 132 (2015);
S. Dulat et al., *Phys. Rev. D* **93**, no. 3, 033006 (2016).
 - [5] H. Abramowicz et al. [H1 and ZEUS Collaborations], *Eur. Phys. J. C* **75**, 580 (2015).
 - [6] M.R. Pelicer et al., *Eur. Phys. J. C* **79**, 9 (2019).
 - [7] D. Schildknecht, *Nucl. Phys. B (Proc. Suppl.)* **99**, 121 (2001);
D. Schildknecht, B. Surrow, M. Tentyukov, *Phys. Lett. B* **499**, 116 (2001);
G. Cvetic, D. Schildknecht, B. Surrow, M. Tentyukov, *Eur. Phys. J. C* **20**, 77 (2001);
N.N.Nikolaev and B.G.Zakharov, *Z.Phys.C* **49**, 607 (1991).
 - [8] M. Kuroda and D. Schildknecht, *Phys. Rev. D* **85**, 094001 (2011);
M. Kuroda and D. Schildknecht, *Int. J. of Mod. Phys. A* **31**, 1650157 (2016).
 - [9] J.J. Sakurai and D. Schildknecht, *Phys. Lett.* **40B**, 121 (1972);
B. Gorczyca and D. Schildknecht, *Phys. Lett.* **47B**, 71 (1973).
 - [10] H. Fraas, B.J. Read and D. Schildknecht, *Nucl. Phys. B* **86**, 346 (1975);
R. Devenish and D. Schildknecht, *Phys. Rev. D* **14**, 93 (1976).
 - [11] D. Schildknecht, in *Proceedings of 8th International Workshop on Deep Inelastic Scattering and QCD (DIS 2000)*, ed. by J.A. Gracey and T. Greenshaw;
G. Cvetic, D. Schildknecht, A. Shoshi, *Eur. Phys. J. C* **13**, 301 (2000);
N.N. Nikolaev and B.G. Zakharov, *Z. Phys. C* **49**, 607 (1991).
 - [12] M.Kuroda and D.Schildknecht, *Phys.Rev.D* **96**, 094013 (2017).
 - [13] G. Altarelli, G. Martinelli, *Phys. Lett. B* **76**, 89 (1978);
A.D. Martin et al., *Phys. Rev. D* **37**, 1161 (1988);
A.M. Cooper-Sarkar et al., *Z. Phys. C* **39**, 281 (1988);
A.M. Cooper-Sarkar et al., *Acta Phys. Pol. B* **34**, 2911 (2003);
R.G. Roberts, *The Structure of the Proton*, (Cambridge University Press 1990).
 - [14] H1 Collab.(V.Andreev et al.), *Eur.Phys.J.C* **74**, 2814 (2014).
 - [15] K. Prytz, *Phys. Lett. B* **311**, 286 (1993).
 - [16] G. R. Boroun, M. Kuroda, and Dieter Schildknecht, *Eur. Phys. J. Plus* **140**, 1149 (2025).